Soil Dynamics and Earthquake Engineering xxx (xxxx) xxx–xxx

Contents lists available at ScienceDirect

Soil Dynamics and Earthquake Engineering

journal homepage: www.elsevier.com/locate/soildyn

LEAP-GWU-2015 centrifuge test at UC Davis

Trevor J. Carey[a,*], Takuma Hashimoto[b,1], Daniel Cimini[a], Bruce L. Kutter[a]

[a] Department of Civil and Environmental Engineering, University of California, Davis, USA
[b] Disaster Prevention Research Institute, Kyoto University, Kyoto, Japan

ARTICLE INFO

Keywords:
LEAP
Centrifuge
Numerical Model Validation
Liquefaction
Modeling

ABSTRACT

For the LEAP-GWU-2015 exercise, a relatively simple centrifuge test was conducted in parallel at 6 centrifuge facilities including the University of California Davis (UCD). The experiment consisted of a submerged medium dense clean sand with a 5° slope subjected to 1 Hz ramped sine wave base motion in a rigid container. This paper explains several details of the experiment at UCD including intended and unintended deviations from the specification and the implementation of new techniques for measurement of saturation of the centrifuge model. One unintended critical deviation was the use of pore fluid that was more viscous than specified; this had significant effect on the pore pressure dissipation time. The other important deviation from the specification was the incomplete ground motion sequence. While it is not ideal for purposes of determining the replicability of centrifuge tests, the differences between experiments diversifies the data available for validation of numerical models.

1. Introduction

Advances in computational power over the last three decades has aided the use of computational methods for geo-mechanical problems. Numerical simulations of the expected deformations and loss of strength of geo-materials during liquefaction has been increasingly incorporated into the design and analysis of complex projects [8]. Although generally trusted, there is no agreed upon technique to evaluate if the numerical models used for liquefaction analysis are correctly predicting the expected response of soil during liquefaction. Previous work such as the (VELACS project) ([1]–1994) have attempted to evaluate numerical simulations, but the findings were inconclusive. LEAP (Liquefaction Experiments and Analysis Projects) as described by [6] is a current collaborative effort to verify and validate numerical liquefaction models.

LEAP will provide high quality laboratory and centrifuge test data to assess the capabilities of constitutive and numerical models. This assessment will be performed over several LEAP exercises (e.g. LEAP1, LEAP2, etc.), each potentially testing different aspects of liquefaction such as those associated with earthen dams, port facilities, or lateral spreading. One such exercise, LEAP-GWU-2015 involved a relatively simple centrifuge experiment performed at six facilities designed to demonstrate repeatability of experimental results. The complete specifications for the LEAP-GWU-2015 centrifuge experiment are provided by Kutter et al. [3] but are briefly discussed herein.

The LEAP-GWU-2015 centrifuge test at UC Davis was performed on the 1 m radius Schaevitz centrifuge at the Center for Geotechnical Modeling. This centrifuge performs 1-D shaking in the plane of spinning requiring the model to have a curved slope as specified by Kutter et al. [3]. This paper will detail the nonconformities from the specification including use of pore fluid with increased viscosity, and an incomplete sequence of ground motions.

2. UC Davis test specific information

2.1. Test specifications

The soil selected for the LEAP-GWU-2015 centrifuge experiment is Ottawa F-65, a clean sand with less than 0.5% fines. Ottawa F-65 was selected for its availability throughout the duration of the LEAP project, and consistent properties (i.e. grain size distribution, particle shape) among batches. The specified target dry density for the experiment is 1652 kg/m^3. According to Kutter et al. [3] this corresponds to a relative density of 65% ± 10%. [2] summarizes index and strength tests for Ottawa F-65 sand.

The Ottawa F-65 sand is specified to be placed with a uniform density and profile, with a 5-degree slope. In prototype scale, the model is specified to be 20 m in length, 4 m deep at the midpoint, and to have a width greater than 9 m. Fig. 1 shows the dimensions of the target model for the UCD centrifuge test to meet the specification. The central

* Corresponding author.
E-mail address: tjcarey@ucdavis.edu (T.J. Carey).
[1] Former Visiting Scholar, Department of Civil and Environmental Engineering, University of California, Davis, USA.

http://dx.doi.org/10.1016/j.soildyn.2017.01.030
Received 21 October 2015; Received in revised form 19 September 2016; Accepted 26 January 2017

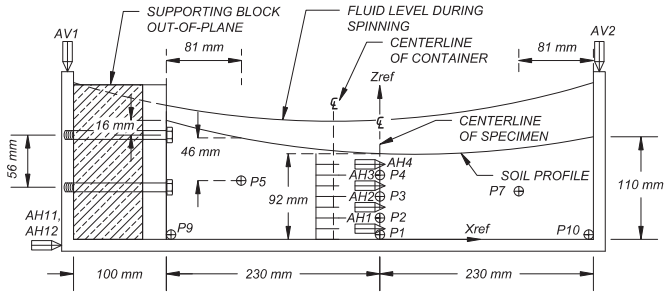

Fig. 1. Dimensions, supporting block location, and sensor layout.

array located at the midpoint along the shaking direction has four accelerometers (AH1-AH4) and four pore pressure transducers (P1-P4). Two additional accelerometers (AH11 and AH12) were included on the container to record the acceleration of the achieved input motion. Two vertical accelerometers are attached to the top of the container to distinguish vertical and rocking accelerations.

The specified ground motion sequence includes five motions, each with a ramped 1 Hz sine wave for 16 cycles. Motions #2 and #4 are destructive with a 0.15*g* and 0.25*g* PGA respectively. Motions #1, #3, and #5 are non-destructive with a PGA of 0.015*g*. Following Motion #2, the centrifuge is specified to be spun down to allow for measurement of surface markers. Following measurement, the centrifuge was to be spun back up and the ground motion sequence completed.

Surface markers were to be placed in a grid pattern on the surface of the soil to measure the deformations during soil liquefaction. The markers are cut zip tie heads measuring 10 mm in length. In addition to measurement at placement, and following Motion #2, the locations of the surface markers were measured following saturation, placement on the arm, and after Motion #5.

2.2. Sensor layout and container modifications

The rigid container at UCD, with the unmodified dimensions of 560 mm (l)×280 mm (w)×180 mm (h) was shortened to 460 mm in length to enable modeling the 20 m length and 4 m depth prototype specification, while accounting for the required curvature of the soil and water surfaces. Fig. 1 details the model scale dimensions, sensor layout, and alterations to the rigid container. The unmodified aspect ratio of length to height in the curved g-field would have resulted in insufficient freeboard and water spilling over the container's end. The container was shortened by 100 mm using a 25 mm thick PVC plate supporting block. The supporting block was braced at 3 locations and bolted to the end walls of the container as shown in Figs. 1 and 2. The block was sealed to prevent drainage along the PVC-container interfaces. The curvature of the model surfaces and corresponding prototype geometry are also illustrated in Fig. 3. The flat base of the container in the radial g-field represents a curved surface in the corresponding prototype, which increases the depth of soil at the container ends, decreasing to the 4 m specified depth at the center. The curved geometry of the model and radial g-field could be considered in numerical simulations of the experiment.

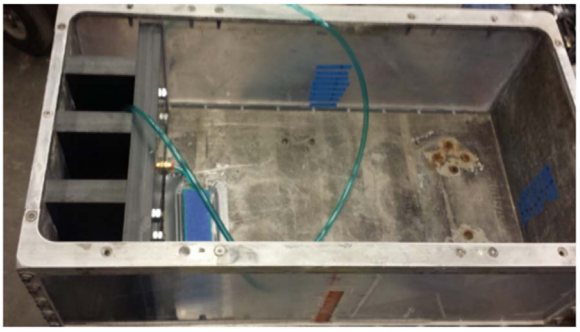

Fig. 2. Photograph of supporting block in the left side of the empty rigid model container.

2.3. Scaling laws

Given the length of the modified container, the scale factor of the slope was determined to be $L^*=L_{container}/L_{prototype}=(0.46\ m)/(20\ m)=1/43.5$. Following Garnier et al. [5] the scale factor for gravity, $g^*=1/L^*=43.5$. The angular velocity of the centrifuge (193 RPM), was calculated to produce 43.5*g* of centrifuge acceleration at a radius of 1.033 m (the radius to 1/3 the depth; 31 mm in model scale below the ground surface at the central array of sensors).

3. As built model

3.1. Achieved density

The Ottawa sand was dry pluviated through a screen attached to the bottom of a hopper, while maintaining a constant drop height of 400 mm. The density produced was calibrated by trial and error adjustments of the pluviation drop height and by blocking portions of the screen to vary the flow rate of sand. The calculated density of soil was 1652 kg/m^3, exactly matching the specification. The thickness of the soil specimen was measured to an accuracy of about 1 mm. A 1 mm error in height would result in approximately 1% error in the density (the soil was about 100 mm thick), and hence the uncertainty in relative density would be about 8% (using $\rho_{d,\ max}$=1750 kg/m^3 and $\rho_{d,\ min}$=1492 kg/m^3) from Kutter et al. [3].

3.2. Approximation of the log-spiral surface

Fig. 4 illustrates the process used to generate the curved slope, approximating the specified 5 degree prototype slope specified by Kutter et al. [3]. The surface of the sand was intended to be inclined at a 5 degree slope from the normal to the radial g-field produced by the centrifuge. Since the radius to the surface varies along the sloped surface, the curvature of the surface would vary along the slope; this shape theoretically is described by a log-spiral. For simplicity, the segment of a log spiral surface was approximated by a tilted circular arc. The change in elevation of the surface from middle of the slope to the top of slope is $(10m)(\tan 5°) = 0.87m$ prototype scale. This corresponds to a radius change of 22 mm for a scale factor of L*= 1/40. For a 1 m centrifuge radius, a 22 mm variation in radius corresponds to a 2.2% maximum deviation between the radius of curvature of the log spiral and the radius of curvature of a circle, justifying the use of a tilted circular arc in place of a log-spiral surface.

The soil was pluviated to cover the desired curve of the surface and then excess soil (approximately 5–10 mm) was removed using a vacuum guided by a tilted circular arc template that rested atop the container. Points along the longitudinal and transverse centerlines were surveyed to check that the depth of the soil was within our attempted tolerance (± 1 mm).

3.3. Viscosity of pore fluid

An error in the calibration of the viscometer resulted in the use of a pore fluid solution that was 10.9 times more viscous than intended. The actual viscosity of the pore fluid in the UCD experiment was 470 centipoise producing a ratio of $\mu^*/g^*=10.9$; while the specified ratio is $\mu^*/g^*=1$, consistent with conventional centrifuge scaling relationships [5]. The increased viscosity significantly affected the rate of dissipation of excess pore water pressures. The pore pressure transducers showed much slower dissipation of excess pore water pressure than the complementing centrifuge experiments (Fig. 9, Kutter et al. [3]).

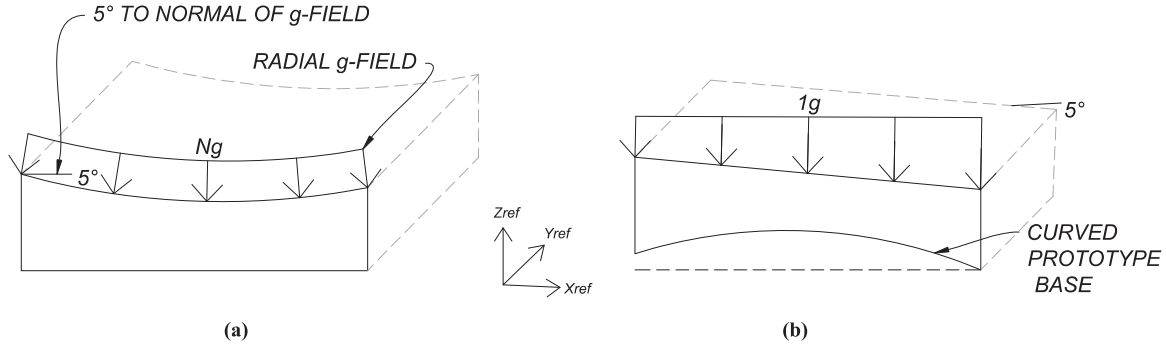

Fig. 3. : (a) Model and (b) prototype geometry of the UCD test.

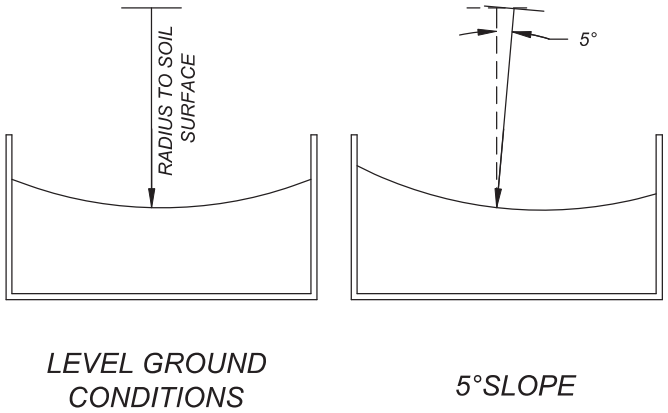

Fig. 4. Curve used to simulate 5° slope for shaking in the plane of spinning.

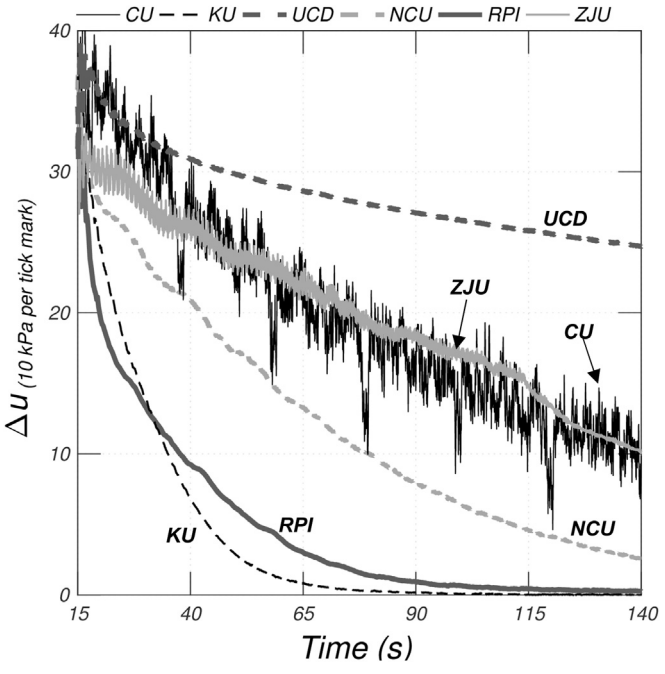

Fig. 5. Excess pore pressure dissipation for P1 of the 6 LEAP-GWU-2015 centrifuge experiments.

Fig. 5 compares the dissipation of excess pore pressure at P1 for the 6 complementing experiments of LEAP-GWU-2015. Over the 125 s shown in Fig. 5, the UCD test roughly dissipates 30% of the pore pressure developed at the end of the strong shaking (Time ~15 s), whereas the complementing experiments dissipated 70–99% of the excess pore pressure generated from strong shaking. The buildup of pore water pressures during strong shaking was also affected, but the effects of increased viscosity are much less apparent because the other models were nearly undrained during shaking anyway.

3.4. Saturation

Prior to saturation, the dry model and container were placed in a large vacuum chamber. The chamber was de-aired with 3 cycles consisting of 15 min of vacuum, followed by 10 min of flooding with carbon dioxide. Following the 3 de-airing cycles, the vacuum was increased to 95 kPa and maintained as methylcellulose pore fluid was dripped onto the surface, where it collected at the bottom of the curved sand surface near the middle of the container and then seeped downward. The drip rate was adjusted to maintain a pool of methylcellulose in the middle of the sample, while keeping the edges dry to allow a path for pore gas to escape. After the soil was completely submerged, the vacuum was released. Due to the high viscosity of the pore fluid, the saturation process took more than 30 h.

The degree of saturation was then checked with a method described by Okamura and Inoue [7]. The vacuum chamber was opened and a device was placed on the fluid surface to measure the change in elevation of the fluid surface and the chamber was resealed. The device, shown schematically in Fig. 6, consisted of two laser pointers attached to the container ends and pointed downward at a five-degree angle from the horizontal towards a measuring tape floating on the surface of the methylcellulose. A small decrease in chamber pressure, Δ_p, was applied and the change in fluid elevation was deduced from the movement of the laser pointer dots on the floating measuring tape. The change in elevation of the fluid surface is presumed to be solely caused by volume change of bubbles trapped in the unsaturated soil. The volume change is also presumed to be uniform over the entire fluid surface. Using Boyle's law shown in Eq. (1), where p_1 is atmospheric pressure (101 kPa), V_{1air} is the volume of air at atmospheric pressure; p_2 is the changed absolute pressure (84 kPa), and V_{2air} is the volume of the bubbles at the changed pressure, the volume of air at atmospheric pressure can be determined. By substituting $p_2=p_1+\Delta_p$, $V_{1air}=V_{1air}+\Delta V_{air}$ in Eq: 1, one may solve for V_{1air} (see Eq: 2). Using the volume of air at ambient pressure (V_{1air}) and volume of water (V_{water}) determined from phase relationships, the degree of saturation ($S_{deg.}$) is solved for with

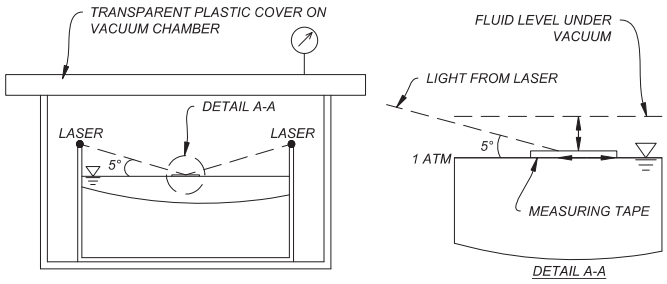

Fig. 6. Method used to check saturation of the centrifuge model inside a vacuum chamber.

Table 1
As-built and after test sensor locations given in prototype scale.

	Specification target coordinates (m)			As built locations – measured (m)			After test coordinates from excavation (m)		
Instrument number	x	y	z	x	y	z	x	y	z
AV1	−14.50	0.00	7.74	−14.50	0.45	7.74	−14.50	0.45	7.74
AV2	10.20	0.00	7.74	10.20	0.41	7.74	10.20	0.41	7.74
AH1	0.00	0.00	0.49	−0.26	0.02	0.49	0.04	0.04	0.40
AH2	0.00	0.00	1.48	0.04	−0.16	1.48	0.30	−0.28	1.41
AH3	0.00	0.00	2.47	−0.05	0.10	2.47	0.20	−0.02	2.03
AH4	0.00	0.00	3.46	−0.22	−0.23	3.46	0.05	−0.56	2.99
AH11	−14.37	4.30	−2.37	−14.37	4.30	−2.37	−14.37	4.30	−2.37
AH12	−14.37	−4.30	−2.37	−14.37	−4.30	−2.37	−14.37	−4.30	−2.37
P1	0.00	1.63	0.15	0.09	−1.56	0.15	0.20	−1.71	0.15
P2	0.00	1.63	0.99	0.33	−1.80	0.99	0.45	−1.84	0.89
P3	0.00	1.63	1.98	0.05	−1.72	1.98	0.09	−1.74	1.76
P4	0.00	1.63	2.97	−0.23	−1.67	2.97	0.06	−1.25	2.77
P5	−6.41	1.63	2.70	−6.53	−1.66	2.70	−6.37	−1.47	2.41
P7	6.41	1.63	2.22	6.35	−1.55	2.22	6.34	−1.68	2.11
P9	−9.74	0.00	0.15	−9.41	−0.06	0.15	−9.41	−0.06	0.15
P10	9.74	0.00	0.15	9.74	−0.06	0.15	9.74	−0.06	0.15

Eq. (3). For the centrifuge test described herein, the degree of saturation was determined to be 99.99%.

$$p_1 V_{1air} = p_2 V_{2air} \tag{1}$$

$$V_{lair}\frac{(p_1+\Delta p)\Delta V_{air}}{-\Delta p} = \frac{(101\ \text{kPa}+(-17\ \text{kPa}))(5\times10^{-5}\text{m}^3)}{17\ \text{kPa}} = 2.5\times10^{-4}\text{m}^3 \tag{2}$$

$$S_{deg.} = \frac{V_{water}}{V_{air}}\times100(\%) = \frac{(1\text{m}^3-2.5\times10^{-4}\text{m}^3)}{2.5\times10^{-4}\text{m}^3}\approx99.99\% \tag{3}$$

3.5. As built sensor locations

Instrument locations, measured during placement and during excavation after testing, are provided in Table 1. The coordinate system is defined in Fig. 1. The difference between as-built and "after test" coordinates of the sensors suspended in soil could be partly due to errors, such as inaccurate measurement, inadvertent tugging on wires after placement or during excavation, and displacement of the sensors relative to the liquefiable soil. The location of the sensors reported in Table 1 is analyzed in Section 5 of this paper to provide displacement vectors.

4. Achieved ground motions

4.1. Horizontal component

The shake sequence for the UCD experiment consisted of five motions summarized in Table 2. The second motion of the sequence, S2 in Table 2 produced a peak acceleration of 0.075*g* and did not meet the specified 0.15*g* for Motion #2. The fourth shaking event of the sequence (S4) was our second attempt to simulate the specified Motion #2 from the experiment specifications, produced a PGA of 0.2*g*.

Table 2
UCD shaking sequence compared to specified ground motion sequence.

UCD Shaking Event Sequence	Corresponding LEAP Spec'd Motion	PGA (g) (LEAP Specified)	PGA (g) UCD 1 Hz component	PGA (g) (UCD)
S1	Motion #1	0.015	0.001	0.058
S2	Motion #2a[a]	–	0.031	0.075
S3	Motion #3	0.015	0.008	0.038
S4	Motion #2	0.15	0.130	0.2
	Motion #4[b]	0.2		
S5	Motion #5	0.035	0.008	0.035

[a] Motion S2, performed at UCD, was not in the LEAP specification
[b] LEAP specified Motion #4 was not accomplished

The achieved base motion for Motions #2a and #2 are compared to the specified acceleration in Fig. 7. To gain insight on the performance of the shaker, the 1 Hz component was isolated by use of a notched band pass filter with corner frequencies of 0.9 and 1.1 Hz. The 1 Hz component was then subtracted from the achieved motion in the time domain, producing a separate record of the high frequency noise component. The 1 Hz component and the high frequency noise component of the achieved motion are shown in Fig. 8. The 0.2*g* PGA of Motion #2 has a significant contributions from higher frequencies; the 1 Hz component of 0.13*g* reasonably matches the specified 0.15*g* for Motion #2. The achieved velocity (obtained by integration of the acceleration record without isolating the 1 Hz component) for Motion #2 follows the specified motion as illustrated in Fig. 9. For these reasons the UCD Event S2 was given the name Motion #2a, and UCD event S4 corresponds to LEAP Motion #2. UCD did not produce a ground motion corresponding to the specified Motion #4.

4.2. Vertical component

The measured vertical motions for Motion #2a and #2 are presented in Fig. 10. The acceleration trace shown at the bottom of the figures is from AV1 and the top trace is from AV2. A fourth order band-pass filter with corner frequencies of 0.3–3 Hz was applied to reduce high frequency noise similar to that described by Kutter et al. [3]. The filtered acceleration is shown in black, whereas the gray is the unfiltered response. The filtered vertical component for Motion #2 has an amplitude of about 19% of the 1 Hz component of the horizontal base. Furthermore, little phase shift between AV1 and AV2 is apparent, an indication that the container was not rocking during shaking.

5. Results

5.1. Pore pressure response

Fig. 11 shows the excess pore pressure response of the central array for Motion #2a and #2. Recall that P1 was at the base of the profile, about 4 m deep, and P4 was about 1 m deep. Using the as-built sensor depths, the initial vertical effective stress at sensors (P1, P2, P3, P4) was approximately 39, 30, 20, and 10 kPa respectively.

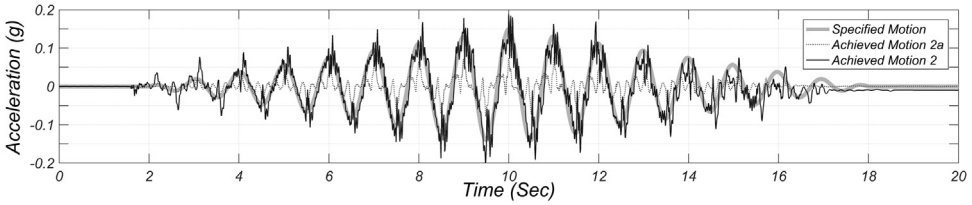

Fig. 7. Achieved and specified acceleration time history for Motions #2 and #2a of the ground motion sequence.

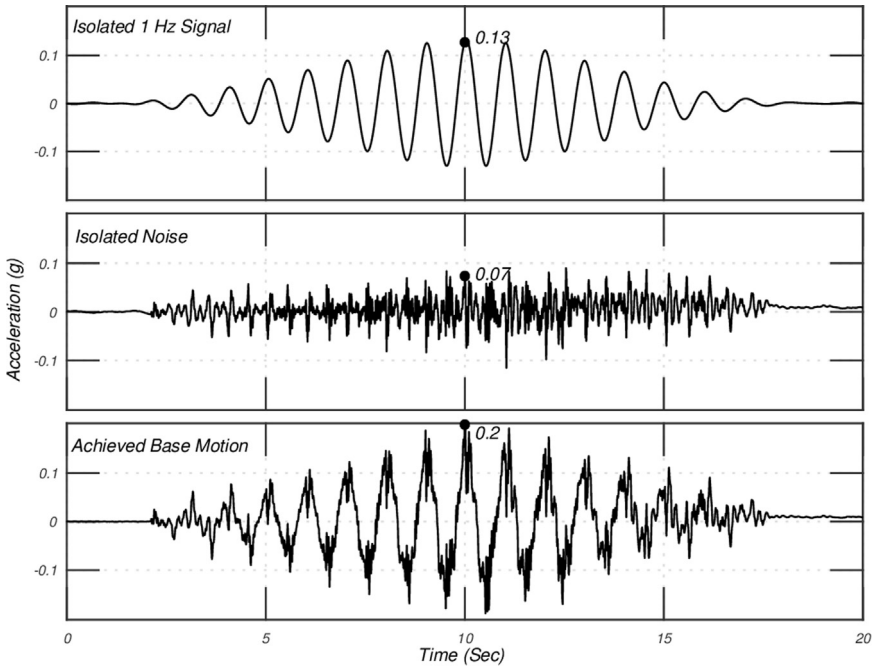

Fig. 8. Achieved base acceleration time history (bottom), high frequency noise isolated from achieved signal (middle), 1 Hz signal (top).

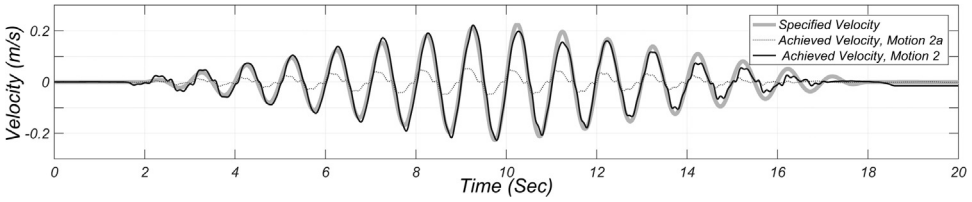

Fig. 9. Achieved and specified velocity time history for Motions #2 and #2a of the ground motion sequence.

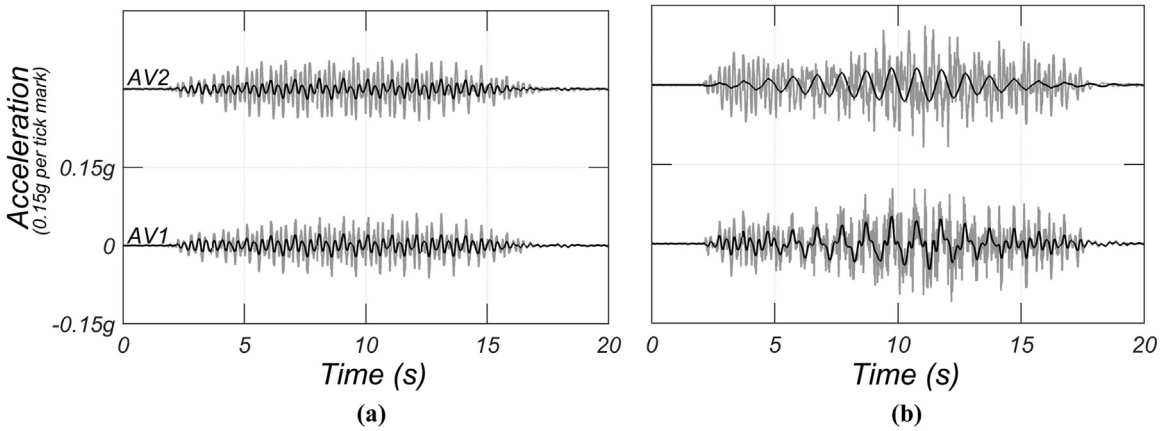

Fig. 10. Vertical acceleration response for: (a) Motion #2a, and (b) Motion #2.

For Motion #2a (Fig. 11a), the soil came close to liquefaction at shallower depths. The pore pressure ratios were approximately 95% at P4, 97% at P3, 66% at P2, and 50% at P1. For Motion #2a, the large pore pressures dissipated relatively rapidly.

For Motion #2 (Fig. 11b), excess pore pressures rapidly build and approach the initial vertical effective stress consistent with the occur-

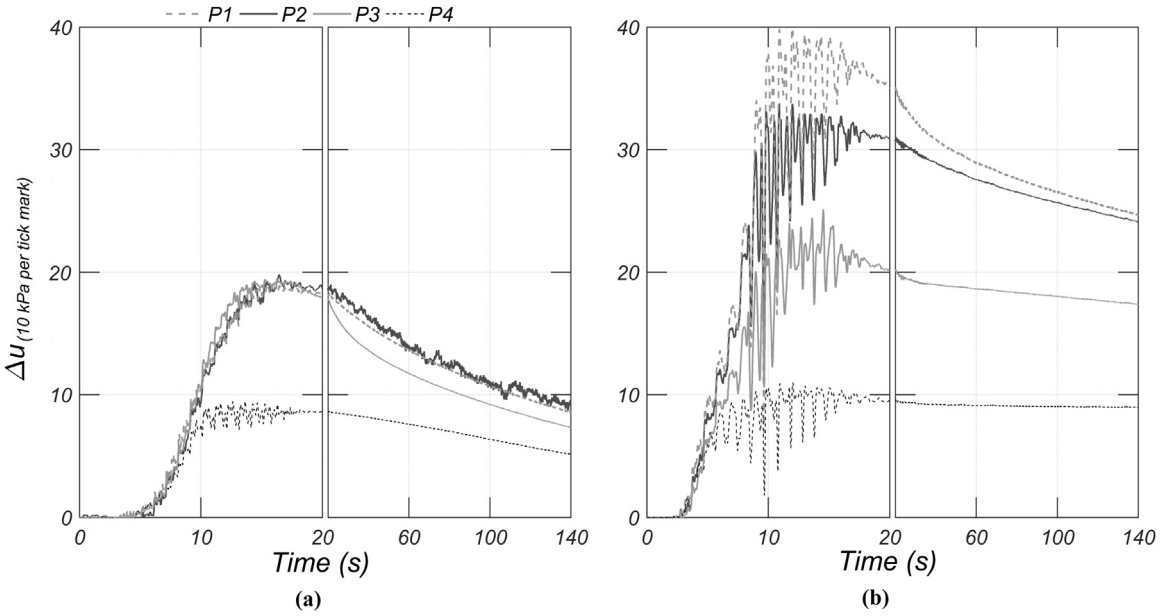

Fig. 11. Pore pressure response of the central array for: (a) Motion #2a, and (b) Motion #2.

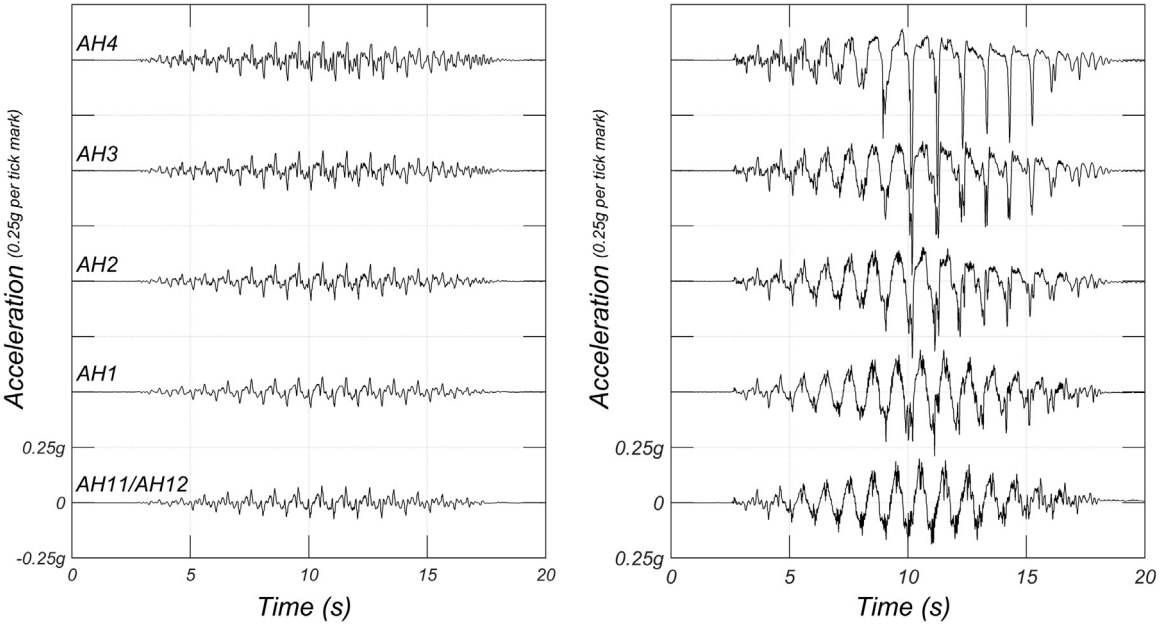

Fig. 12. Acceleration response of the central array for: (a) Motion #2a, and (b) Motion #2.

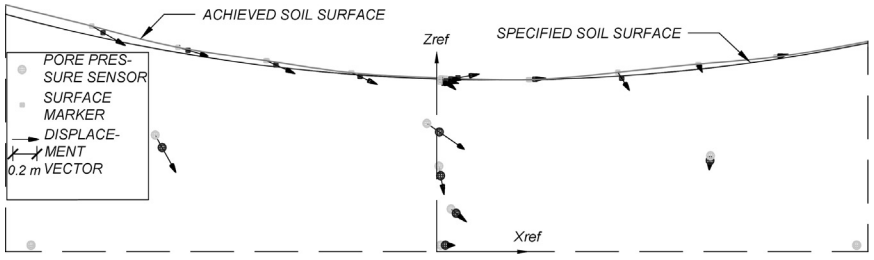

Fig. 13. An elevation view of surface maker and pore pressure sensors locations prior to the first and following the last spin (without magnification). Vectors show the displaced path, magnified 3 times.

rence of liquefaction. Excess pore pressures measured at the shallower sensors (e.g. P4, P3) reach their respective initial effective confinement stress first and remained at that pressure a longer duration after the shaking amplitude decreased. After excess pore pressures reached the initial effective vertical stress, sharp spikes began to appear, which is consistent with the dilatancy that is triggered when large strains occur in liquefied soil. The spikes are described as deliquefaction shock waves [4].

The deeper sensors begin to dissipate first following strong shaking. The shallower sensors show little to no dissipation over the time

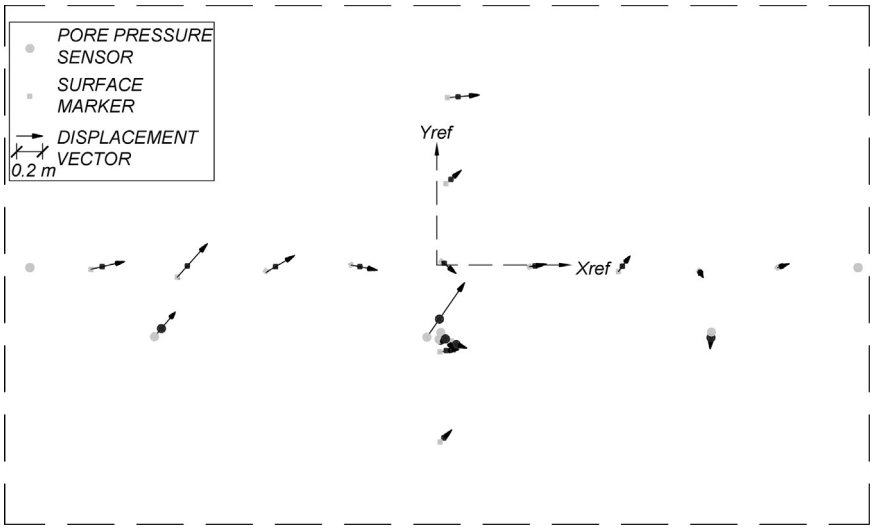

Fig. 14. A plan view of surface maker and pore pressure sensors locations prior to the first and following the last spin (without amplification). Vectors show the displaced path, magnified by 3 times the measured displacement.

considered. Therefore, the shallow layers must maintain excess pore pressures longer.

5.2. Acceleration response

Motion #2a and #2 acceleration time histories for the central array are shown in Fig. 12. The base motion AH11/AH12 followed by AH1-AH4 are plotted from bottom to top, in the same sequence as constructed in the model.

For Motion #2a, the trace of accelerations for the base motion and central array are very similar and largely in phase, indicating that the soil was moving almost as a rigid mass and only small shear strains accumulated in the model.

For Motion #2 (Fig. 12b), initially, the recorded accelerations in the soil profile follow the trace of the achieved base motion. Following the initiation of liquefaction, which is characterized with the sharp deliquefaction spikes, the waveform significantly changes both in frequency and amplitude from the base motion. The deviations from the motion follow the progression of liquefaction, and the sensors near the surface deviate first followed by the sensors near the bottom of the container. The amplitude of the acceleration spikes are greatest near the ground surface where the soil liquefied first and where the pore pressure ratios were the greatest.

5.3. Surface maker response

Fig. 13 (elevation view) and 14 (plan view) shows the initial and final locations of the surveys of the surface maker grid and the pore pressure transducers. The initial surface marker locations were obtained following model placement on the centrifuge arm. The final locations of the surface makers were obtained following the sequence of the ground motions, prior to removal of the model from the centrifuge arm. Displacement vectors connect the initial to the final locations but are magnified by a factor of 3.(Fig. 14).

The average x displacement of the pore pressure sensors is approximately 0.2 m and the corresponding settlement is approximately 0.3 m. These values agree with the UCD surface displacements both in magnitude and direction as indicated by the displacement vectors. The horizontal and vertical displacements of the surface markers tend to be greater in the upper part (left side) of the slope and smaller nearer the bottom (right side) of the slope.

6. Conclusion

This paper describes the performance and results from the UC Davis centrifuge test for LEAP-GWU-2015. The logic for curving the surface of the model is explained in some detail, and a new technique used to measure the degree of saturation was also explained.

The experiment is useful for validation of numerical models and for assessment of the replicability of experiments at different facilities. For each of these uses it is important that the degree of compliance between the specified experiment and the performed experiment are understood. The base motion for Motion #2 velocity closely matched the specification for Motion #2. The PGA of the base acceleration, including the high frequency components of the motion is larger than the specification, but the isolated 1 Hz component was slightly smaller, and closely matched the specification for Motion #2. A small shaking event, Motion #2a, was performed prior to Motion #2. While Motion #2a is also useful for validation, it was not part of the specification and could result in discrepancies between results from other facilities.

The other major nonconformity of the UC Davis experiment was that the pore fluid was 10.9 times more viscous than it was specified to be. Of course, this should be accounted for if this data is to be used for validation proposes. The results of the experiment showed liquefaction occurred during Motion #2. The excess pore water pressures measured at P1-P4 approached the initial effective vertical stress, indicating liquefaction. The pore pressure sensors displayed spikes of negative pore pressure consistent with the cycle deliquefaction triggered by cyclic dilatancy. The acceleration records of the central array showed that very small strains were developed during Motion #2a. In Motion #2, small strains were observed in the beginning of the ground motion, but after liquefaction developed, the acceleration records became spiky, consistent with the sudden transition between soft behavior when pore pressures are high and stiff behavior when the dilatancy triggers pulses of negative pore pressure (i.e., pulses of increased effective stress) called “deliquefaction”. The spikey behavior was not observed in Motion #2a.

The distribution of the deformations in the model are illustrated by plotting displacement vectors from surface markers and pore pressure sensors. These plots give some idea of the deformation patterns as well as the uncertainty in the measurements of the sensor and marker locations. Movements indicated settlement and some downslope lateral spreading. The movements tended to be greater in the upper part of the slope and smaller in the lower part of the slope (near the bottom wall of the rigid model container).

Acknowledgements

This experiment and the planning phase of the LEAP project was supported by National Science Foundation (NSF) under Grant No. CMMI-1344630. The authors would like to thank the staff at the Center for Geotechnical Modeling (CGM) for their assistance and technical insight throughout the test.

References

[1] Arulanandan K, Scott RF. editors. Verification of numerical procedures for the analysis of soil liquefaction problems. A.A. Balkema; 1993.
[2] Carey TJ, Kutter BL, Manzari MT, Zeghal M, Vasko A. LEAP soil properties and element test data. DOI: 10.17603/DS2WC7W; 2015.
[3] Kutter BL, Carey TJ, Hashimoto T, Zeghal M, Adboun T, Kokkali P, Madabhushi G, Haigh S, Burali d' Arezzo F, Madabhushi S, Hung WY, Lee CJ, Chegn HC, Iai S, Tobita T, Zhou YG, Chen Y, Sun ZB, Manzari MT. Leap-GWU- experiment specifications, results, and comparisons. Soil Dynamics and Earthquake Engineering (this issue); 2017.
[4] Kutter BL, Wilson DW. De-liquefaction shock waves. In: Proceedings of the seventh US–Japan workshop on earthquake resistant design of lifeline facilities and countermeasures against soil liquefaction, Seattle. p. 295–310; 1999.
[5] Garnier J, Gaudin C, Springman SM, Culligan PJ, Goodings DJ, Konig D, Kutter BL, Phillips R, Randolph MF, Thorel L. Catalogue of scaling laws and similitude questions in geotechnical centrifuge modelling. Int J Phys Model Geotech 2007;8(3):1–23.
[6] Manzari MT, Kutter BL, Zeghal M, Iai S, Tobita T, Madabhushi SPG, Haigh SK, Mejia L, Gutierrez DA, Armstrong RJ. LEAP projects: concept and challenges. : In: Proceedings of the fourth international conference on geotechnical engineering for disaster mitigation and rehabilitation (4th GEDMAR): 2014 Sept 16-18; Kyoto, Japan: Taylor and Francis; 2015.
[7] Okamura M, Inoue T. Preparation of fully saturated model for liquefaction study. Int J Phys Model Geotech 2012;12(1):39–46.
[8] Perlea VG, Beaty MH. Corps of Engineers practice in the evaluation of seismic deformation of embankment dams. In: Proceedings of the Fifth international conference on recent advances in geotechnical earthquake engineering and soil dynamics May 24-29; San Diego, CA; 2010.